Construction and Building Materials 307 (2021) 124328

Contents lists available at ScienceDirect

Construction and Building Materials

journal homepage: www.elsevier.com/locate/conbuildmat

Effect of casting and curing temperature on the interfacial bond strength of epoxy bonded concretes

Dana Daneshvar, Karl Deix, Agathe Robisson *

Research Group of Building Materials and Technology, Institute of Material Technology, Building Physics and Building Ecology, Faculty of Civil Engineering, Vienna University of Technology (TU Wien), Karlsplatz 13/207-01, A-1040 Vienna, Austria

ARTICLE INFO

Keywords:
Concrete-concrete bonding
Casting and curing temperature
Bond strength
Epoxy adhesive
Setting time

ABSTRACT

The effect of casting and curing temperature on concrete-epoxy-concrete interfacial bond strength was evaluated. To cover a wide range of climatic conditions, six different temperature values from 5 to 55 °C were considered. The interfacial bond strength of the composites was experimentally assessed using pull-off, wedge splitting and bi-surface shear tests. The individual materials, epoxy and cement paste, were also characterized by means of viscosity, shore D hardness and setting time measurements. Results show that the casting and curing temperature dramatically impacts the mechanical properties of the epoxy bonded concretes. Indeed, increasing temperature from 5 to 55 °C leads to a decrease in bond strength up to 65%. The significant drop in setting time of epoxy compared to cement at high temperature, the inferior epoxy mechanical properties, as well as the reduction in epoxy thickness due to material loss in pores and microcracks can explain this decrease.

1. Introduction

Concrete-to-concrete composites have been increasingly used in a wide range of applications including buildings, bridges, roads and dams. These composites are mainly used to strengthen/repair existing structures, construct precast to cast-in-place joint members and fabricate multi-material composites [1–3]. The concrete-concrete interface is generally treated as a weak point and critical area owing to the material discontinuity, high pore accumulation, and micro-crack concentration [4,5]. Relative slippage, debonding and delamination are among the most common issues, causing weak bond strength and non-monolithic response to loads [6,7]. A robust interfacial bond between concrete members is an essential requirement to ensure the effectiveness of concrete-concrete composites. In this regard, studies have identified numerous factors influencing the performance of interfaces, namely the substrate surface condition (roughness, moisture, cracking) [1,8–11], the concrete type and mechanical properties [12–15], the mechanical crossing reinforcement [16–18], the environmental conditions (temperature, freeze thaw cycles, etc.) [19,20] and the use of bonding agents [13,17,21–23]

Epoxy resin is one of the most commonly used bonding agents to provide a better adhesion between concrete layers and thus enhance the bond strength [1,24,25]. The effectiveness of epoxy adhesives relies on its application method, concrete surface state and environmental conditions [17,26]. Temperature is a key factor affecting the interfacial bond of the epoxy bonded concrete composites, as their constituents behaviors show a great temperature dependence [19]. Epoxy, as an individual material, cures faster at high temperature [27,28]. It was shown that for curing temperatures higher than 5 °C, the curing duration required to achieve the ultimate strength of the resin is halved for every 10 °C increase [29]. Curing temperature does not only influence the rate of stiffness and strength development, but also impacts its ultimate mechanical properties in a non-monotonic way. Specifically, increasing the curing temperature up to the glass transition temperature (T_g) may lead to a greater strength and stiffness, but upon exceeding the T_g, the mechanical properties begin to decay as a consequence of the increase in randomness of the adhesive crosslinking network, oxidative crosslinking and degradation of the polymer structure [28,30–32].

Concrete performance is also dependent on the weather condition [33–35]. Studies have shown that employing a casting and curing temperature above 40 °C can negatively impact the concrete mechanical properties, namely elastic modulus, fracture energy, compressive, tensile and flexural strengths [36–39]. At temperatures above 40 °C, the hydration of Portland cement is not only accelerated, but the nature, stability, morphology and apparent density of the hydration products are also modified. Additionally, these high temperatures may result in a

* Corresponding author.
E-mail addresses: dana.daneshvar@tuwien.ac.at (D. Daneshvar), karl.deix@tuwien.ac.at (K. Deix), agathe.robisson@tuwien.ac.at (A. Robisson).

https://doi.org/10.1016/j.conbuildmat.2021.124328
Received 13 March 2021; Received in revised form 12 July 2021; Accepted 20 July 2021

non-homogeneous dispersion of hydration products inside the hardened cement paste pores that leads to a porous structure within the cement paste [36,40,41]. Moreover, upon extended curing, the layer of C-S-H phase that forms around the C_3S surfaces is dense, and hinder their hydration, reducing the degree of hydration and the ultimate strength at elevated temperatures (above 40 °C) [40,42]. It must be pointed out that the exothermic hydration process of cement can induce temperature rises up to 100 °C in massive concrete-concrete composites [43–45].

The epoxy bonded concretes are exposed to various temperatures depending on climate conditions and heat produced by cement hydration. Although the effect of temperature during casting/curing has been explored on individual components, its impact on the composite properties has not been thoroughly investigated so far. Therefore, this research aims at evaluating the effect of casting and curing temperature on the interfacial bond strength of epoxy bonded concrete layers. For this purpose, six different temperature values from 5 to 55 °C were considered, representing a wide range of climatic conditions at which epoxy bonded concrete composites are built. The interfacial bond strength of the conditioned composites was then tested under pull-off, wedge splitting and bi-surface shear tests, representing various states of stress applied to the interface in real field conditions. The characterization of both epoxy and cement paste properties, as individual materials, were also conducted as a function of temperature by means of viscosity (epoxy), shore D hardness (epoxy) and setting time (cement) assessments.

Performing this experimental study aims at bringing a deeper insight into the properties of epoxy bonded concretes by quantifying their bond performance under a large range of casting and curing temperatures. Eventually, such quantification will help refine design recommendations of epoxy bonded concretes.

2. Materials and methods

2.1. Materials

2.1.1. Concrete

A concrete strength class of C30/37 was used. All the concrete mixtures were prepared with the *DER CONTRAGRESS* ordinary Portland cement (CEM I 42.5 N, C_3A free), following the mix design presented in Table 1. The average 28-day cube compressive strength of concrete was measured equal to 44.4 ± 2.8 MPa.

2.1.2. Epoxy

A commercial epoxy bonding agent (*BASF MasterTop P 604*) was used. The adhesive was prepared by mixing the resin (bisphenol A epichlorohydrin) with the amine-based hardener, using the recommended mass ratio of 100:27. The properties of the components and the resulting epoxy were provided by the manufacturer and are listed in Table 2. Quartz sand, with a median particle size (D50) of 343 μm, was added to the mixture to increase its viscosity and mitigate immediate dripping/sagging of the epoxy while applying and curing [46]. The presence of sand may also enhance the bond strength [19]. The mass ratio of quartz sand to the mixture of resin-hardener was 1:1, equivalent to a sand volume percentage of 35%. The density of the resulting bonding agent (epoxy + quartz sand) was measured equal to 1.85 g/cm^3.

Table 1
Mix proportions of concrete substrate and overlay.

Ingredient	(kg/m^3)
Cement	300
Water (W/C=0.6)	180
Aggregate [0-1 mmm]	573.8
Aggregate [1-4 mmm]	286.9
Aggregate [4-8 mmm]	306
Aggregate [8-16 mmm]	746

Table 2
Epoxy characteristics as provided by the manufacturer.

Properties		
Density (at 23 °C)	Part A (resin)	1.62 g/cm^3
	Part B (hardener)	1.02 g/cm^3
	Mixed (Epoxy)	1.44 g/cm^3
Viscosity (at 20 °C)	Part A (resin)	9500 mPa.s
	Part B (hardener)	80 mPa.s
	Mixed (Epoxy)	1400 mPa.s
Glass transition temperature (T_g)	Mixed (Epoxy)	44 °C
Compressive strength (after 28 days)	Mixed (Epoxy)	55 MPa
Tensile strength (after 7 days)	Mixed (Epoxy)	10 MPa

2.2. Concrete-concrete composites preparation

Six concrete slabs with dimensions of 50 × 25 × 6 cm^3 were cast and cured for 28 days in the lab ambient conditions (average temperature of 23 °C and relative humidity of 50%). A shot blasting surface treatment was then applied. This commonly used procedure consists in shooting tiny steel shots at high velocity against the concrete surface, roughening the concrete surface and removing contaminants all at once (see Fig. 1). The mean texture depth of the final surface was measured equal to 0.6 mm using the sand patch test method in accordance with EN 1766. Additionally, the pore size distribution of the cast slabs was measured through the Mercury Intrusion Porosimetry (MIP). The porosity was equal to 14.2% and the average and median pore diameters were equal to 29 and 76 nm, respectively.

The surface treated substrates were then stored three months in the lab under ambient conditions.

In the next step, a wide range of typical in-situ casting temperatures were simulated. For this purpose, climate chambers were used to expose the constituents of the composites to the studied temperatures, namely 5, 15, 25, 35, 45, 55 °C (humidity was not controlled). All constituents of the concrete composites, i.e., substrates, bonding agent components (resin, hardener, and quartz sand) and concrete overlays components (aggregate, cement, water) were placed in the climate chambers pre-set at the given temperature. After 24 h of temperature exposure, the components of epoxy were taken out of the climate chambers and mixed. The same amount of epoxy mixture, i.e. 230 g, was then spread uniformly on each substrate using a hand roller, see Fig. 2. Assuming that all the epoxy is placed uniformly on the substrate surface (50 × 25 cm^2), the thickness of epoxy layer is calculated to be 1 mm. Simultaneously, the components of concrete overlay were also taken out of the climate chamber and mixed. In less than two minutes, the concrete overlay was then poured and spread on top of the epoxy layer (See Fig. 2(b)). After compacting and floating, the final thickness of overlay was equal to 3 cm in all composites.

The concrete-concrete composite specimens were then covered with plastic sheets to minimize drying shrinkage and placed back into their respective climate chambers. After 7 days of curing, the composite specimens were taken out of the climate chambers and further cured in the lab ambient conditions (average temperature of 23 °C and relative humidity of 50%) for 21 days. Fig. 3 shows the schematic of the final composite specimen (50 × 25 × 9.1 cm^3) prepared for each studied temperature. The specific samples required for each test method were cut out of these composites and tested as described in the section 2.3.

Note that the difference in coefficients of thermal expansion (CTE) of the epoxy and concrete likely induces residual stresses in the epoxy layer

Fig. 1. Concrete surface treatment of substrate slabs: **(a)** shot blasting; **(b)** steel shots (average diameter of 1.8 mm); **(c)** rough substrate surface.

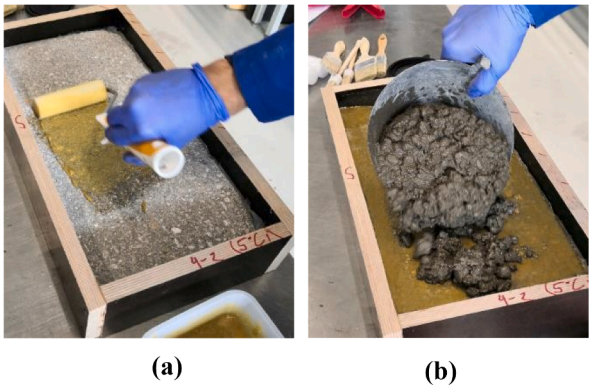

Fig. 2. Composite slab preparation: **(a)** epoxy bonding agent spreading on concrete substrate; **(b)** placing concrete overlay.

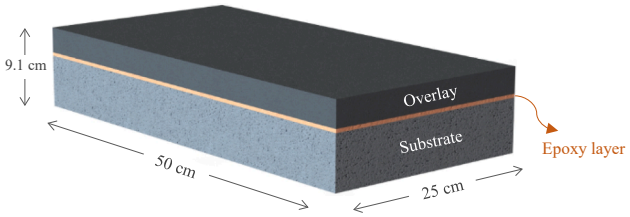

Fig. 3. Schematic of concrete-concrete composite slab specimen.

upon bringing the specimen back to room temperature. Using estimated CTEs of epoxy and concrete, the maximal residual stress was estimated to be around 8 MPa. However, previous studies have shown that this residual stress does not influence the interfacial toughness [47], and this aspect will not be discussed further.

2.3. Test methods

Various test methods have been developed over the years to characterize the interfacial bond strength. The main difference among these tests is the stress applied to the interface, resulting in different values of bond strength. It was shown that the bond strength can be varied by a factor of 8 depending on the type of test method [48]. In this study, three different methods were used to characterize the interfacial bond strength. All tests were performed in the lab ambient condition (average temperature of 23 °C and relative humidity of 50%). In addition to the bond tests, the properties of both epoxy and cement paste were assessed, individually. Each test method is described below.

2.3.1. Pull-off test

The pull-off test measures the strength of the bond subjected to a tensile load. Due to its simplicity, this test can be used both for laboratory and on-site assessments. In this study, 5 cm wide cores were drilled 5 cm into the composites (2 cm below the interface), see Fig. 4. Four replicates were tested for each studied temperature. The pulling tests were carried out with a monotonic loading rate of 50 N/s using a *Proceq* pull-off tester. As shown in Fig. 4, the pulling force is applied through the glued steel dollies, allowing to pull on the core with a force that is perpendicular to the interface. The interfacial bond strength under pulling force was then calculated using the measured value of failure (maximum) tensile force divided by the surface area of the core. It must be pointed out that the pull-off test generally gives the most conservative bond strength results, as there is no contribution from interfacial friction [48].

2.3.2. Wedge splitting test

The wedge splitting test (WST) was originally introduced by Linsbauer & Tschegg [49] and was further developed by Brühwiler & Wittmann [50]. It has been widely used to measure the fracture properties of quasi-brittle materials, including concrete. Stable crack growth, small sample size, easy load application and minimized elastic energy stored in the testing machine are the main advantages of WST [50,51]. Here, the WST samples were $10 \times 9 \times 8$ cm^3 prisms, and a starter notch with a 2 cm length was sawed along the interface, resulting in an 8 cm long ligament, as shown in Fig. 5. Four replicates were tested for each studied temperature. The samples were subjected to loading through a monotonic vertical crosshead displacement rate of 0.2 mm/s using a *Zwick* 250 kN testing machine. The vertical compressive load (F_v) and crack mouth opening displacement (CMOD) were measured by means of a 100 kN load cell and two LVDT gauges, respectively.

In this test, the stiff wedge is pushed down and the roller bearings convert the vertical compressive load into a horizontal splitting load (F_h), inducing the Mode I fracture, see Fig. 5. The friction between wedge and rollers is deemed negligible (<1%) and the vertical component of the load on the rollers is low [52]. Considering the wedge tip angle ($\alpha = 7.5^{\circ}$), the splitting force (F_h) can be calculated from the vertical load (F_v) using the equation (1):

$$F_h = \frac{F_v}{(2\tan\alpha)} \tag{1}$$

The specific fracture energy (G_f) can be calculated using the work of fracture (W_f) (area under the F_h-CMOD curve) divided by the projected

fracture area (ligament area A_{lig}), as described in equation (2):

$$Gf = \frac{W_f}{A_{lig}} = \frac{1}{B(W-a_0)} \int F_h d\delta_h \quad (2)$$

Where, W is sample depth; a_0 is initial notch length; B is sample thickness; F_h is splitting load and δ_h is the horizontal displacement of the load point (CMOD).

The nominal notch tensile strength (σ_{NT}) is a parameter that contains the effect of both tensile and flexural stresses applied in the ligament of the specimen. The (σ_{NT}) is calculated using the maximum splitting load ($F_{h,\max}$), as provided in the equation (3):

$$\sigma_{NT} = \frac{F_{h,max}}{B(W-a_0)} \left(1 + \frac{6y}{(W-a_0)}\right) \quad (3)$$

Where, y is the vertical distance between the center of gravity of the ligament area and the horizontal force.

2.3.3. Bi-surface shear test

The bi-surface shear test was first applied to concrete by Momayez et al. [53], and is used to evaluate the bond strength under pure shear stress. Compared to other shear test methods, this test has advantages such as symmetrical loading, ease of fabrication and closer simulation of real stress state in the field [53]. In this study, test samples were 9 × 5 × 5 cm^3 prisms with the overlay-to-substrate height ratio of 1:2. A starter notch with a length of 1.5 cm was sawed along the interface to enforce that the shear failure plane occurs there. Three replicates were tested for each studied temperature. The sample rested on two identical steel plates separated by a distance equal to the steel plate placed on the top-middle of the sample. The compressive load was applied through the top steel plate, inducing two shear planes, one located along the interface and the other one within the substrate, see Fig. 6. The shear bond strength is calculated by taking half of shear force at failure (maximum value) divided by the vertical shear plane surface area.

2.3.4. Epoxy viscosity and hardness measurement

The viscosity of epoxy samples was measured at studied temperatures, namely 5, 15, 25, 35, 45, 55 °C. Two types of samples were prepared, one with epoxy only and the other containing quartz sand, as used for the production of the concrete samples. The reaction of the resin and hardener is rapid at elevated temperatures, especially above 40 °C, and accompanied by a further self-acceleration caused by the exothermic heat of reaction [28,54]. To slow down the rate of reaction between mixing and testing, the epoxy mixture was placed, right after mixing, in a bucket filled with ice. An *Anton-Paar MCR 302* torque-controlled rotational rheometer was used, with a 25 mm plate–plate

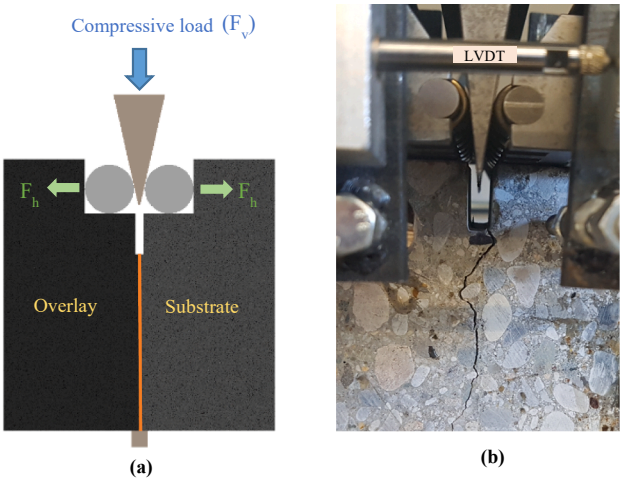

Fig. 5. Wedge splitting test: **(a)** schematic of sample and loads; **(b)** detailed test setup.

geometry. The gap between plates was chosen equal to 0.5 and 2 mm for the epoxy and epoxy-quartz sand samples, respectively. In the latter case, the gap was more than 5 times bigger than the median particle size (D50) of the quartz sand (343 μm) in order to get bulk rheological properties. The Peltier-temperature-controlled hood was used to get uniform temperature. Because of the fast curing reaction, the test had to be performed as quickly as possible. Therefore, the lower plate and hood were first pre-set to the adjusted temperature and then, depending on the type of sample, 2.5 ml of epoxy or 10 ml of epoxy-quartz sand were placed on the lower plate. The gap was then adjusted and the temperature-controlled hood was placed. A waiting time of 60 s was selected to provide enough time for the sample to reach the desired temperature value, while trying to avoid further reaction of the epoxy. Finally, upon starting the test, the shear rate was gradually ramped up from 1 s^{-1} to 100 s^{-1} enabling the measurement of epoxy viscosity as a function of shear rate.

Additionally, the shore D hardness of the epoxy was measured to follow its hardness evolution and treated as a measure of curing time window. Epoxy samples were prepared from single components equilibrated at the given temperature, cast in the silicone molds (68 × 37 × 15 mm^3) and cured at the studied temperatures, i.e. 5, 15, 25, 35, 45, 55 °C, for 7 days. Shore D hardness was measured during these 7 days by means of *PCE-DX-DS* Shore D hardness tester. For each measurement, the sample was taken out from the climate chamber, 5 indents were

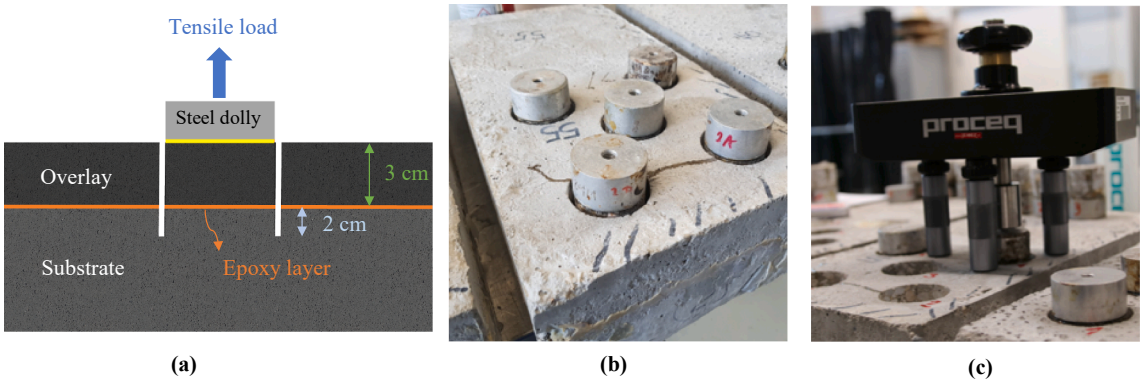

Fig. 4. Pull-off test: **(a)** core specification; **(b)** alignment of cores and glued steel dollies; **(c)** pull-off tester.

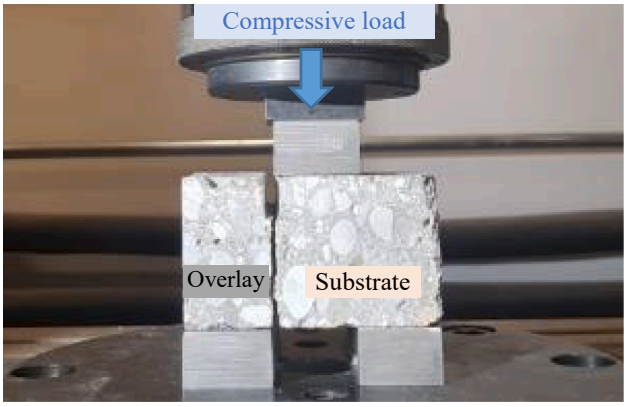

Fig. 6. Bi-surface shear test setup.

performed on different spots and their average and standard deviation were reported. Between measurements, the sample was returned to the climate chamber to continue the curing process. After 7 days, the samples were taken out of the climate chambers and kept in the lab ambient condition for 21 more days (like composites were) and the shore D hardness was measured again at the end of this stage. In total, the shore D hardness measurement lasted 4 weeks during which the epoxy experiences temperature conditions similar to the ones experienced within the composite. Using the hardness measurement versus time, the epoxy initial and final curing times were defined. The initial curing time, sometimes called open time, is the time period during which the epoxy remains liquid (shore D hardness of zero). The open time is an important indicator of the time that epoxy remains workable enough to be spread on surfaces. The final curing time was defined as the time it takes for epoxy to reach 90% of its 7-day shore D hardness value.

2.3.5. *Cement paste setting time*

Parallel to epoxy characterization, the initial and final setting times of the cement paste were determined using *Controls automatic Vicamatic-2* (model 63-L2700/PR). The needle diameter was 1.13 mm and penetrations were automatically performed at intervals of 10 min. Following the same W/C used for the concrete composites, the cement paste samples were prepared from water and cement conditioned at the studied temperature value, and then poured into the 40 mm high truncated mold with upper and lower diameter of 65 and 75 mm, respectively. The filled mold was placed in the container and then the water was added such that the surface of cement paste sample is submerged to a depth of 0.5 mm. A thermo silicone heating foil connected to the thermostat was placed in the water container to maintain the sample temperature at the studied temperatures (25, 35, 45, and 55 °C) while hydrating. For low temperatures (5 and 15 °C), the whole test setup was placed in the preset climate chamber and measurements were conducted there. According to the standard EN 196–3 [55], the initial setting time is defined as the time between the cement paste mixing and the time when the distance between the tip of penetrating needle and the base plate reaches 6 ± 3 mm. The final setting time is defined when the needle first penetrates only 0.5 mm into the cement paste sample.

2.3.6. *Interface microscopy*

The microstructures of epoxy bonded concretes were characterized using both optical and scanning electron microscopy techniques. For the optical microscope measurements, small prism samples ($6 \times 3 \times 2$ cm^3) were cut from the concrete-concrete composites such that the interface was located in the middle of cross section, see Fig. 7(a). Samples were impregnated with a slow setting epoxy to enable the grinding and polishing of their surfaces using a *Struers LaboPol-60* machine. The cross section of samples was first grinded on *Struers MD-Piano* diamond discs with grit size of 80, 220, 500, 1200, successively, and then polished on cloth discs, namely *MD-Sat*, *MD-Mol*, *MD-Nap* using abrasive diamond suspensions of 6, 3 and 1 μm, successively. The optical micrographs of the polished samples were analyzed through ImageJ software. Using the image segmentation technique, the epoxy adhesive layer was detected and highlighted in yellow-orange color, as shown in Fig. 7(b). Computing the area of highlighted zone divided by the length of the sample gives the mean thickness of set epoxy spread along the concrete-concrete interface.

Back Scattered Electron (BSE) imaging was used to observe

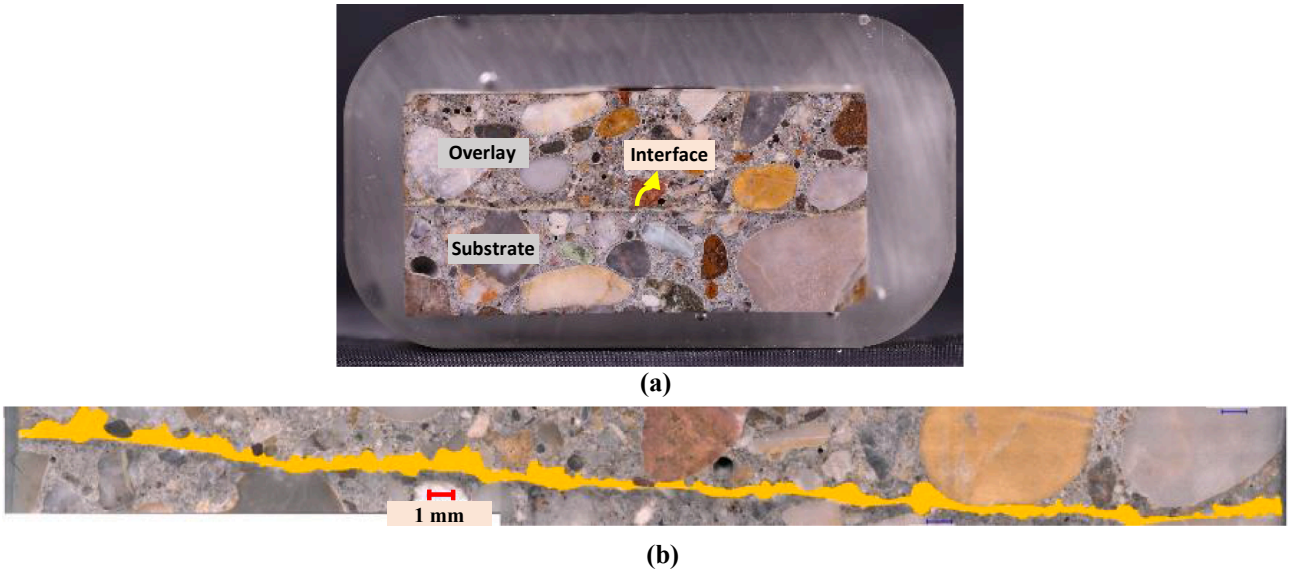

Fig. 7. Epoxy layer characterization: (a) image of polished sample; (b) highlight of epoxy layer from optical micrograph (image segmentation).

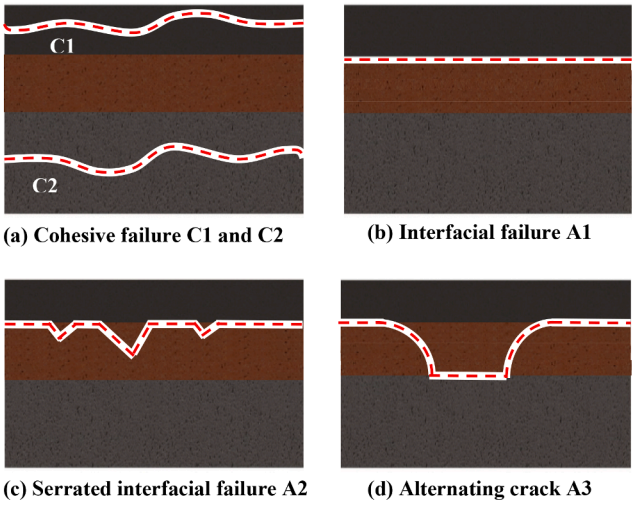

Fig. 8. Schematic of different failure modes based on crack path locations. The red dashed lines represent the main crack path approximate location.

the microstructures of cement based materials with the advantage of distinguishing the constituting phases based on their atomic number, such as hydrated cement pastes, anhydrous cement pastes, microcracks, pores, ITZ and aggregates [41,56,57]. In this study, backscattered electron 2D-images of the interface and its near areas were captured using a Scanning Electron Microscope (SEM: *Philips XL 30 series*) . The SEM scan operating at 12 kV was performed on prism samples ($2 \times 2 \times 1$ cm^3) cut out of the composites.

3. Results and discussion

3.1. Observations of failure locations

Depending on the location of the main observed crack paths, failure modes were classified into two major groups, namely cohesive and adhesive failures [47]. In cohesive failure mode, the failure occurs within the bulk concrete, either in the overlay or substrate, denoted by (C1) and (C2), respectively (see Fig. 8.(a)). Cohesive failure is usually considered representative of a successful bonding, demonstrating the greater strength of the interfacial bond compared to that of bulk concrete. The adhesive failure mode includes three failure paths, namely interfacial failure between the epoxy layer and overlay (A1), serrated interfacial failure (A2), and alternating crack (A3), as shown in Fig. 8(b-d).

3.2. Pull-off test

Pull-off test results are listed in Table 3. It must be pointed out that in the case of cohesive failure, the failure tensile stress only gives an underestimation of bond strength and the value is used as a conservative estimate.

The average failure tensile stress is plotted as a function of temperature in Fig. 9. The result indicate that the casting and curing temperature highly impacts the bond strength. Namely, increasing the temperature from 5 to 55 °C results in lowering the tensile bond strength from 2.35 ± 0.15 to 0.85 ± 0.07 MPa, i.e., a 64% reduction in bond strength. The consistency of the test results is determined by comparing the coefficients of variation (COVs) differing in the range of 6.6% to 22.2% with an average of 11.8%. Hence, the low dispersion confirms the reliability of the results.

The one-way analysis of variance (ANOVA) was performed to evaluate whether there are significant differences between the means. Moreover, the Post Hoc Tukey-Kramer test was also employed to identify where the significant differences lie between each specific pair of groups. Given the variation of tensile bond strength with temperature, the results of ANOVA and Tukey's pairwise statistical analysis are presented in Table 4. The p-value of 1.1E-09 statistically shows that at least one group among studied temperatures presents a significant difference from the others with a confidence level of 95% (p-value < 0.05). Given the Post Hoc Tukey-Kramer test, the absolute difference results are listed in Table 5 with a critical range of 0.44. If the absolute difference exceeds the critical value, it shows that there is a significant difference between the means of that paired groups. Except for the pairs (T5-T15, T5-T25, T15-T25, and T45-T55), a significant reduction (highlighted in bold and asterisk) in tensile bond strength has occurred upon increasing the casting and curing temperature. Tukey's results revealed that the effects of low temperatures (5, 15, and 25 °C) on the loss of failure tensile stress were not significantly different from each other. Also, the effect of temperature of 45 °C was not found to be significantly different than that of 55 °C.

Fig. 10 shows typical post-mortem pull-off samples, illustrating the different failure modes observed. The cohesive failure was the predominant type of failure in the 5 and 15 °C samples, indicating that the tensile strength of the bond is greater than that of the bulk concrete used in the overlay and substrate. However, for the casting and curing temperatures above 15 °C, the majority of failures were adhesive. The shifting of the failure location from interface to bulk concrete when temperature decreases clearly demonstrates the higher interfacial bond strength at low temperatures.

3.3. Wedge splitting test (WST)

Maximum splitting loads and specific fracture energies with varying temperatures were calculated from splitting load-CMOD measurements, and listed in Table 6. Results show that peak splitting loads are greater at low temperatures. For instance, the average maximum splitting load of the 5 °C sample is 2.2 times greater than the 55 °C one. The average WST specific fracture energy function of temperature is plotted in Fig. 11. Here again, in the case of cohesive failure, the reported specific fracture energy values only give a lower estimation of the interfacial bond strength and should only be used as a conservative value. The results demonstrate once more the great effect of casting and curing temperature. Indeed, increasing the temperature from 5 to 55 °C results in lowering the WST specific fracture energy from 111 ± 20.7 to 38.9 ± 8.9 N/m, i.e., a 65% reduction in Mode I specific fracture energy. The COVs range from 5.5% to 33%, with an average of 17.1% showing a larger data dispersion in the WST compared to that of the pull-off test. In all samples, consistent crack mouth opening displacement was measured by two LVDTs connected to both sides of samples, and is reliable. The larger data dispersion could originate from the notch sawing process, inducing microcracking near the notch.

Table 7 shows the analysis of variance (ANOVA) at 95% confidence level yielded a p-value of 3.6E-10 for WST specific fracture energy results, demonstrating that there is a statistically significant difference in at least one group among the six groups of studied temperatures. Given Tukey's test, the absolute difference results are listed in Table 8. with a critical range of 27. Tukey's statistical analysis shows that the WST specific fracture energy is significantly reduced (highlighted in bold and asterisk) upon increasing the casting and curing temperature, except for the pairs (T5-T15, T35-T45, T35-T55, and T45-T55). It means that the effects of high temperatures (35, 45, and 55 °C) on the loss of the WST specific fracture energy were not significantly different from each other. Also, the influence of temperature between 5 °C and 15 °C was not found to be significant.

Inconsistent with other test results, the specific fracture energy is found larger at 25 °C than at 5 and 15 °C. To explain this result, the

Table 3
Pull-off test results.

Curing and casting temperature (°C)	Sample ID	Failure tensile stress (MPa)	Average (MPa)	Standard deviation (MPa)	COV (%)	Failure mode
5	P5-1	2.56	2.35	0.15	6.6	C2
	P5-2	2.29				C1
	P5-3	2.36				C1
	P5-4	2.20				C1
15	P15-1	2.18	2.44	0.21	8.5	C1
	P15-2	2.37				C2
	P15-3	2.61				C1
	P15-4	2.60				C2
25	P25-1	2.38	2.06	0.23	11.2	A3
	P25-2	1.94				A2
	P25-3	1.85				A1
	P25-4	2.05				A3
35	P35-1	1.36	1.54	0.23	14.9	A1
	P35-2	1.37				A1
	P35-3	1.84				A1
	P35-4	1.57				A1
45	P45-1	0.80	1.06	0.24	22.2	A1
	P45-2	0.92				A1
	P45-3	1.24				A1
	P45-4	1.28				A1
55	P55-1	0.95	0.85	0.07	7.7	A1
	P55-2	0.80				A1
	P55-3	0.84				A1
	P55-4	0.83				A1

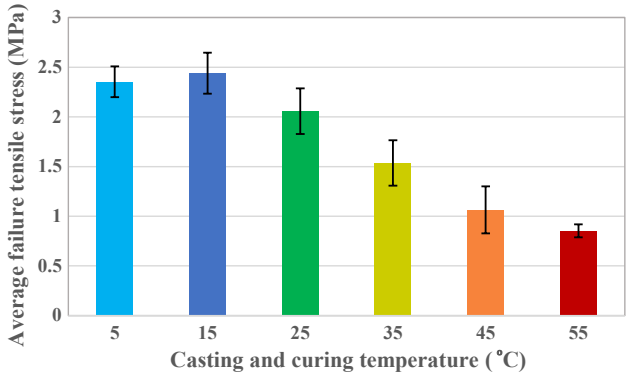

Fig. 9. Average failure tensile stress measured with pull-off test function of casting and curing temperature. Error bars represent standard deviation.

Table 4
Analysis of Variance (ANOVA) of pull-off test results.

Source of Variation	*SS*	*Df*	*MS*	*F*	*P-value*	F_{crit}
Between Groups	8.9	5	1.8	46.6	1.1E-09	2.8
Within Groups	0.7	18	0.04			
Total	9.7	23				

SS: sum of squares; df: degrees of freedom; MS: mean square; F: local factor; p-value: probability value; Fc: critical factor

Table 5
Tukey's pairwise statistical analysis of pull-off test results.

	Absolute difference					
	T5	T15	T25	T35	T45	T55
T5	–	0.1	0.3	**0.8***	**1.3***	**1.5***
T15		–	0.4	**0.9***	**1.4***	**1.6***
T25			–	**0.5***	**0.9***	**1.2***
T35				–	**0.5***	**0.7***
T45					–	0.2
T55						–

* Significant difference

average values of nominal notch tensile strength (σ_{NT}) and ratio of (G_f/σ_{NT}) were calculated (Table 9). Results show that in spite of higher maximum splitting load and nominal notch tensile strength, the (G_f/σ_{NT}) ratio is lower in the 5 and 15 °C samples than in the 25 °C one. A lower ratio of (G_f/σ_{NT}) is typically observed in more brittle materials [58]. Here, the greater brittleness behavior at 5 and 15 °C is attributed to the crack deviation into the bulk concrete, which exhibits a quasi-brittle behavior. On the other hand, adhesive serrated interfacial and alternating crack failure observed at 25 °C (see Fig. 8 and Fig. 13) induce a more dissipative fracturing process. Indeed, the localization of the fracture within the epoxy, with crack deflection from one side to the other, results in higher energy dissipation (increased toughness), specifically in the initial part of softening curve. The mean splitting load-CMOD curves plotted Fig. 12 confirm this explanation.

At temperatures of 35 °C and higher, all failures but one happened at the interface between epoxy and overlay, resulting in low fracture energies. This finding is in line with the results of previous studies [59].

Typical post-mortem WST samples are shown in Fig. 13. As in pull-off samples, the majority of observed failures at 5 and 15 °C are cohesive, while adhesive failures are the predominant failure modes observed at higher temperatures. This confirms the fact that at low temperatures (5 and 15 °C), the interfacial bond is strong enough.

3.4. Bi-surface shear test

Individual and average results of the bi-surface shear tests are shown Table 10. Compared to the pull-off test results, greater bond strength values are reached for all samples, an increase mainly attributed to the contribution of interfacial friction to load carrying. In contrary to pull-off and wedge splitting tests, all failures were adhesive. Representative failure surfaces are shown in Fig. 14. Enforcing the fracture to occur along the interface was a benefit of the notched bi-surface shear test as it permitted to determine the shear bond strength at all studied temperatures, i.e. all fractures are adhesive.

Results plotted in Fig. 15 show that the shear bond strength decreases from 5.8 ± 0.34 to 3.65 ± 0.34 MPa when temperature increases from 5 to 55 °C, i.e. a 37% reduction in interfacial bond strength. The decrease is less significant than that of pull-off and WST results, demonstrating the lower impact of casting and curing temperature on the shear bond

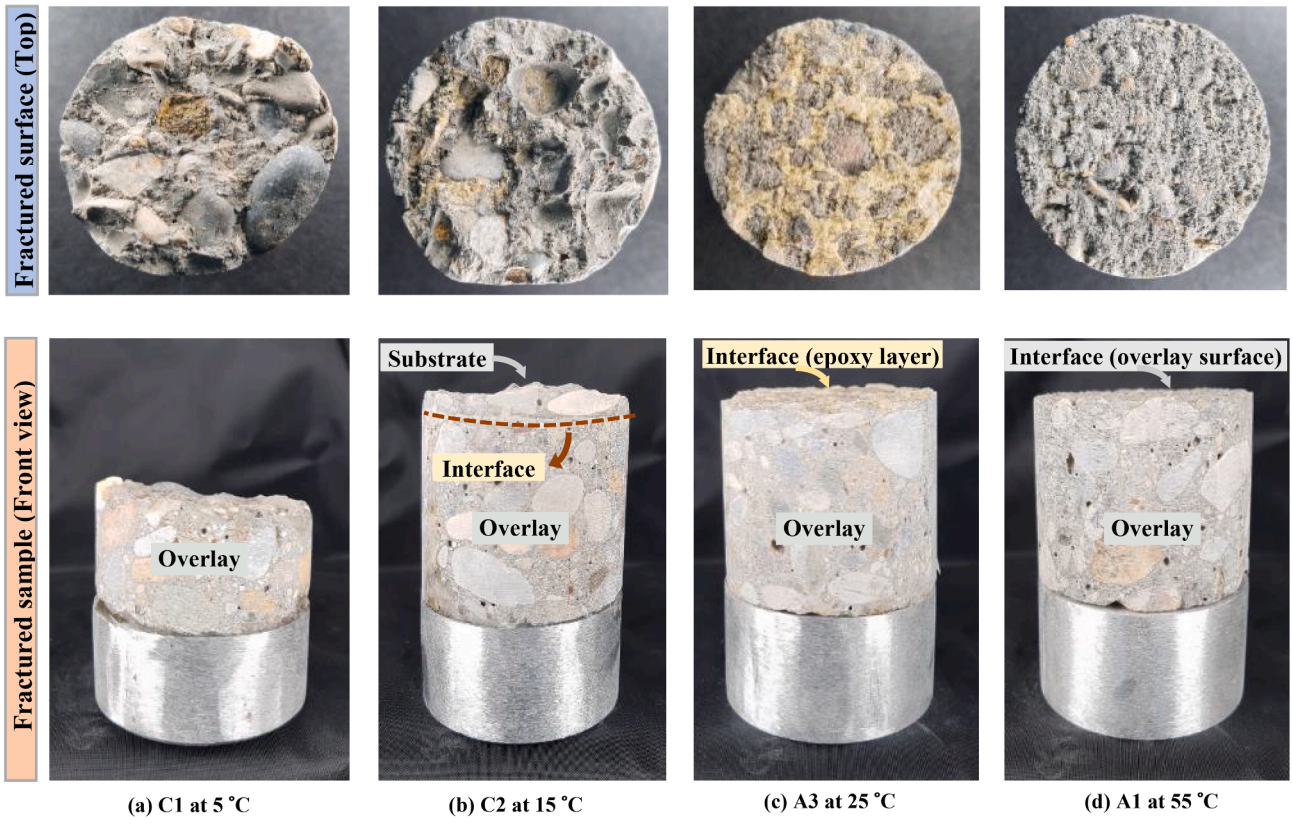

Fig. 10. Representative post-mortem pull-off test samples, highlighting different failure modes. The (C1) and (C2) represent the cohesive failure in the concrete overlay and substrate, respectively. The (A3) indicates the adhesive alternating crack failure and (A1) shows the adhesive interfacial failure between the epoxy layer and overlay.

Table 6
Wedge splitting test results.

Curing and casting temperature (°C)	Sample ID	Maximum splitting load (kN)	Average (kN)	Specific fracture energy (N/m)	Average (N/m)	Standard deviation (N/m)	COV (%)	Failure mode
5	W5-1	3.02	2.98	141.5	111	20.7	18.6	C1
	W5-2	2.94		106.4				C2
	W5-3	3.25		98.2				C2
	W5-4	2.71		98.0				C1
15	W15-1	2.87	3.23	93.9	104.6	12.1	11.6	C2
	W15-2	3.42		120.0				C2
	W15-3	3.19		96.0				C1
	W15-4	3.46		108.3				C2
25	W25-1	2.61	2.64	140.0	140.4	7.7	5.5	A2
	W25-2	2.76		149.5				A3
	W25-3	2.54		130.8				A2
	W25-4	2.64		141.1				A3
35	W35-1	1.78	1.8	61.3	55.7	6.1	10.9	A1
	W35-2	2.08		59.8				A1
	W35-3	1.86		53.6				A1
	W35-4	1.46		48.0				A3
45	W45-1	1.20	1.19	29.5	33.2	10.9	33	A1
	W45-2	1.03		20.9				A1
	W45-3	1.12		35.4				A1
	W45-4	1.40		47.1				A1
55	W55-1	1.20	1.35	32.1	38.9	8.9	22.8	A1
	W55-2	1.44		32.4				A1
	W55-3	1.41		40.2				A1
	W55-4	1.56		50.9				A1

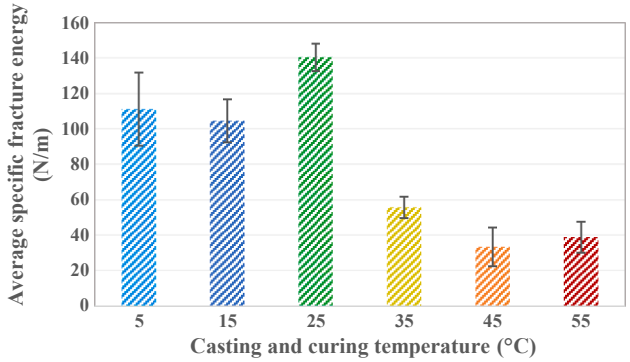

Fig. 11. Average specific fracture energy measured with WST function of casting and curing temperature. Error bars represent the standard deviation.

Table 7
Analysis of Variance (ANOVA) of WST test results.

Source of Variation	*SS*	*df*	*MS*	*F*	*P-value*	F_{crit}
Between Groups	38681.7	5	7736.3	53.5	3.6E-10	2.7
Within Groups	2604.8	18	144.7			
Total	41286.5	23				

SS: sum of squares; df: degrees of freedom; MS: mean square; F: local factor; p-value: probability value; Fc: critical factor

Table 8
Tukey's pairwise statistical analysis of WST results.

	Absolute difference					
	T5	T15	T25	T35	T45	T55
T5	–	6.5	**29.3***	**55.3***	**77.8***	**72.1***
T15		–	**35.8***	**48.9***	**71.3***	**65.7***
T25			–	**84.7***	**107.1***	**101.5***
T35				–	22.5	16.8
T45					–	5.7
T55						–

* Significant difference

Table 9
Fracture parameters measured with WST for the samples cast and cured at 5, 15, and 25 °C.

Casting temperature (°C)	5	15	25
Peak splitting load (kN)	2.98	3.23	2.64
Nominal notch tensile strength (MPa)	3.18	3.14	2.83
Specific fracture energy (N/m)	111	104.6	140.4
G_f/σ_{NT} (mm × 10^{-3})	34.9	33.5	49.8
Failure mode	Cohesive	Cohesive	Adhesive A2

G_f: specific fracture energy; σ_{NT}: nominal notch tensile strength.

strength. According to the shear-friction theory, interfacial friction contributes to shear strength, besides the interfacial cohesion brought by the epoxy adhesive [60,61]. Interfacial friction is mainly governed by surface roughness, which is not impacted by temperature, explaining the lower temperature dependency of the shear bond strength. The gained COVs range between 5.9% and 10.5%, with an average of 8.3%. Therefore, the narrow range of COV values in this test is an indication of the consistent reproducibility of the obtained results.

The corresponding ANOVA statistical analysis results are listed in Table 11 for the bi-surface shear test results. The p-value of 0.03 indicates that there is at least a significant difference between a group of studied temperatures to the others at 95% confidence level. In the Tukey's test, the critical range was determined to be 2.1 and the absolute difference results are shown in Table 12. It can be seen that there is a significant reduction (highlighted in bold and asterisk) of shear bond strength when low casting and curing temperatures (5, 15, and 25 °C) are increased to 55 °C. For the other pairs, no significant difference was found.

3.5. Epoxy characterization

It is clear that the epoxy adhesive plays a pivotal role in the interfacial bond strength. Any change in epoxy properties, both during casting and after, would impact the bond strength of epoxy bonded concretes. Below are presented the results of the epoxy characterization, as an individual material, carried out as a function of temperature.

3.5.1. Viscosity

Both the epoxy and the epoxy-quartz sand samples exhibit a slightly shear-thinning behavior between shear rates of 1 and 100 s^{-1} at all temperatures. Viscosity as a function of temperature was therefore arbitrarily plotted at a shear rate of 50 s^{-1}. Fig. 16 shows that the viscosities of the epoxy and epoxy-quartz sand samples decrease by a factor 12 and 5, respectively, when temperature increases from 5 to 55 °C. Moreover, as expected, the epoxy samples containing quartz sand (35 vol%) show greater viscosity at all temperatures compared to that of epoxy samples. Adding quartz sand therefore provides two advantages: it increases viscosity at all studied temperatures and lowers the effect of temperature (the decrease of viscosity with temperature is less).

3.5.2. Thickness after curing of composites

The mean thickness of epoxy measured on the composites after 28 days of curing is presented in Fig. 17. Given the initial amount of epoxy applied, and assuming no epoxy is lost to cracks or pores, the epoxy thickness was expected to be 1 mm. Results reveal, however, that the

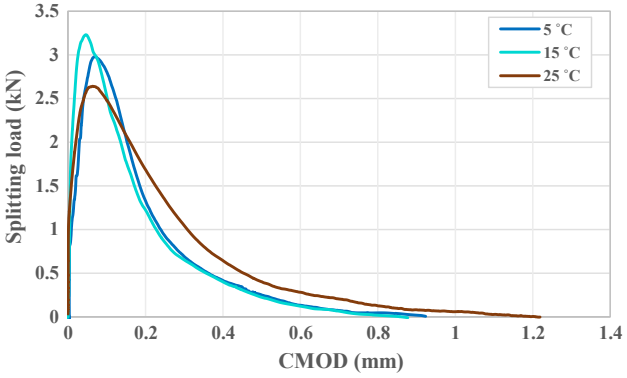

Fig. 12. Splitting load-CMOD curves measured with WST for samples cast and cured at 5, 15, and 25 °C. Each curve is built by averaging loads at a given CMOD of four samples.

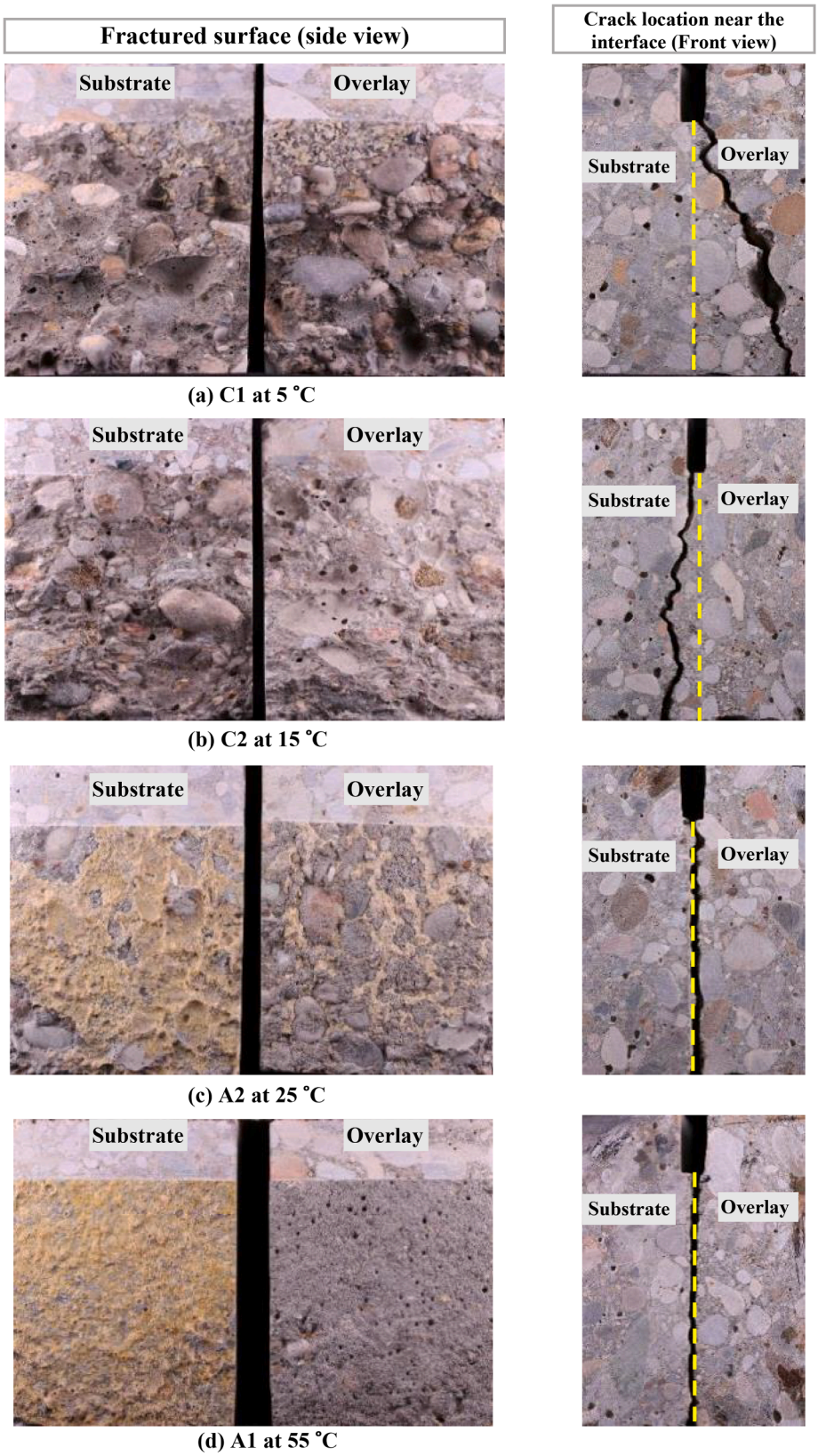

Fig. 13. Representative post-mortem WST samples. The (C1) and (C2) represents the cohesive failure in the concrete overlay and substrate, respectively. The (A2) indicates the adhesive serrated interfacial failure and (A1) shows the adhesive interfacial failure between the epoxy layer and overlay, respectively. The yellow dashed lines highlight the interface approximate location.

Table 10
Bi-surface shear test results.

Casting Temperature (°C)	Sample ID	Failure shear stress (MPa)	Average (MPa)	Standard deviation (MPa)	COV (%)	Failure mode
5	S5-1	6.16	5.8	0.34	5.9	A3
	S5-2	5.74				A2
	S5-3	5.49				A2
15	S15-1	6.43	5.84	0.52	8.8	A3
	S15-2	6.42				A3
	S15-3	4.67				A2
25	S25-1	6.30	6.44	0.37	5.7	A2
	S25-2	6.70				A3
	S25-3	6.34				A2
35	S35-1	4.79	5.34	0.56	10.5	A1
	S35-2	5.03				A1
	S35-3	6.21				A1
45	S45-1	2.74	4.5	0.43	9.6	A1
	S45-2	5.18				A1
	S45-3	5.56				A1
55	S55-1	2.56	3.65	0.34	9.4	A1
	S55-2	4.63				A1
	S55-4	3.75				A1

epoxy thickness is smaller than expected at all temperatures. Furthermore, the mean thickness of epoxy decreases upon rising curing temperature, with the average thickness reduced from 0.74 mm at 5 °C to 0.33 mm at 55 °C, showing a greater escape/loss of epoxy from the interface at elevated casting and curing temperatures. It is likely that the inadequate thickness of adhesive layer negatively impacts the bond strength [26].

Backscattered electron images (BSE) of the interface confirm that employing higher casting and curing temperature leads to penetration of epoxy into the substrate, filling the pores and micro-cracks (see Fig. 18). The factor 10 drop in viscosity of epoxy between 5 and 55 °C can easily explain this result. Previous results have also shown that lower viscosity epoxy could fill deeper and smaller pores [62], and that a greater escape/loss of epoxy from the interface was one of the reasons behind a weaker interfacial adhesion, and hence weaker bond strength between concrete layers [26]. It must be emphasized that although the magnitude of epoxy penetration depth could be attributed to the viscosity, the fast curing time (open time) of epoxy also plays a pivotal role in the epoxy distribution near the interface. Fig. 18(c) shows that only 316 μm of a 400 μm deep micro crack has been filled by the epoxy. It is likely that the rapid hardening of epoxy stopped a deeper penetration into the concrete substrate. A more detailed discussion about the effect of temperature on the epoxy open time is provided in the next section.

3.5.3. Shore D hardness

The evolution of shore D hardness of the epoxy samples with time, for the first 7 days of curing under different temperatures, is plotted in Fig. 19. As the curing process proceeded, the epoxy hardness evolved with a rate highly dependent on the curing temperature. Slow but continuous development of shore D hardness is observed for the samples cured at low temperatures (5 and 15 °C), whereas high curing temperatures lead to a very fast hardening (setting), followed by a steady-state region. After 7 days of curing (the plateau region), the low shore D hardness values of 65 and 48, measured at 45 and 55 °C, respectively, are linked to temperature being near or above the glass transition temperature of epoxy (specified to be 44 °C by the manufacturer).

Epoxy shore D hardness measured at 28 days of curing (7-day temperature curing plus 21-days lab ambient condition curing) is plotted in Fig. 20. The epoxy samples cured at high temperatures exhibit lower hardness values at 28 days. Specifically, the shore D hardness values of the epoxy cured at 45 and 55 °C are 71 ± 1.45 and 62 ± 1.2, respectively, which are 5.8% and 17.8% lower than the average shore D hardness of the samples cured between 5 and 35 °C (75.4). The reduction in epoxy ultimate shore D hardness, as well as other mechanical properties [63,64], with increasing temperature has been linked to the increase in randomness of the adhesive crosslinking network, oxidative crosslinking and degradation of the polymer structure at high curing temperatures [28,30]. It is very likely that the epoxy cured within the composite would exhibit the same decrease in mechanical properties with setting temperature than when cured individually. The reduction in mechanical properties of epoxy at high curing temperatures could be another reason explaining the decrease in interfacial bond strength of epoxy-bonded concretes with increasing curing temperature.

3.6. Setting times of epoxy and cement paste

It has been shown that chemical and physical interactions develop between epoxy polymer molecules and hydration products of ordinary Portland cement (OPC), strengthening the interface [65]. Therefore, it is likely that the setting of epoxy before the hydration products of cement are present would negatively affect the epoxy-concrete bond. The initial and final setting times of cement paste and epoxy (with the same recipes to those used in composites) were therefore measured (See Fig. 21). As expected, the temperature influences both the epoxy and cement paste setting time. Specifically, upon increasing temperature from 5 to 55 °C, the epoxy open time (initial curing) decreases sharply from 20 h to 15 min. Moreover, while 107 h are required for the epoxy to reach 90% of its 7-day shore D hardness (final curing) at 5 °C, only 35 min are needed at 55 °C. Cement paste setting time also decreases with temperature. At 5 °C, the initial and final setting times are 25 and 37 h, and they drop to about 6 and 8 h at 55 °C. The time gap between these initial and final setting times shows the region during which the setting process is ongoing (See Fig. 21). The graph clearly shows the setting time windows of epoxy and fresh overlay barely overlap at 35, 45 and 55 °C, reducing the likelihood of proper physical and chemical interactions between overlay and epoxy. Indeed, fractures are, in all cases, adhesive at these temperatures.

Further analyzing the differential setting times, the epoxy degree of curing was plotted as a function of the initial and final setting times of cement paste, see Fig. 22. The epoxy degree of curing was defined as the ratio between the shore D hardness at the considered time and the 7-day (plateau) shore D hardness. Results show that in samples cured at lower

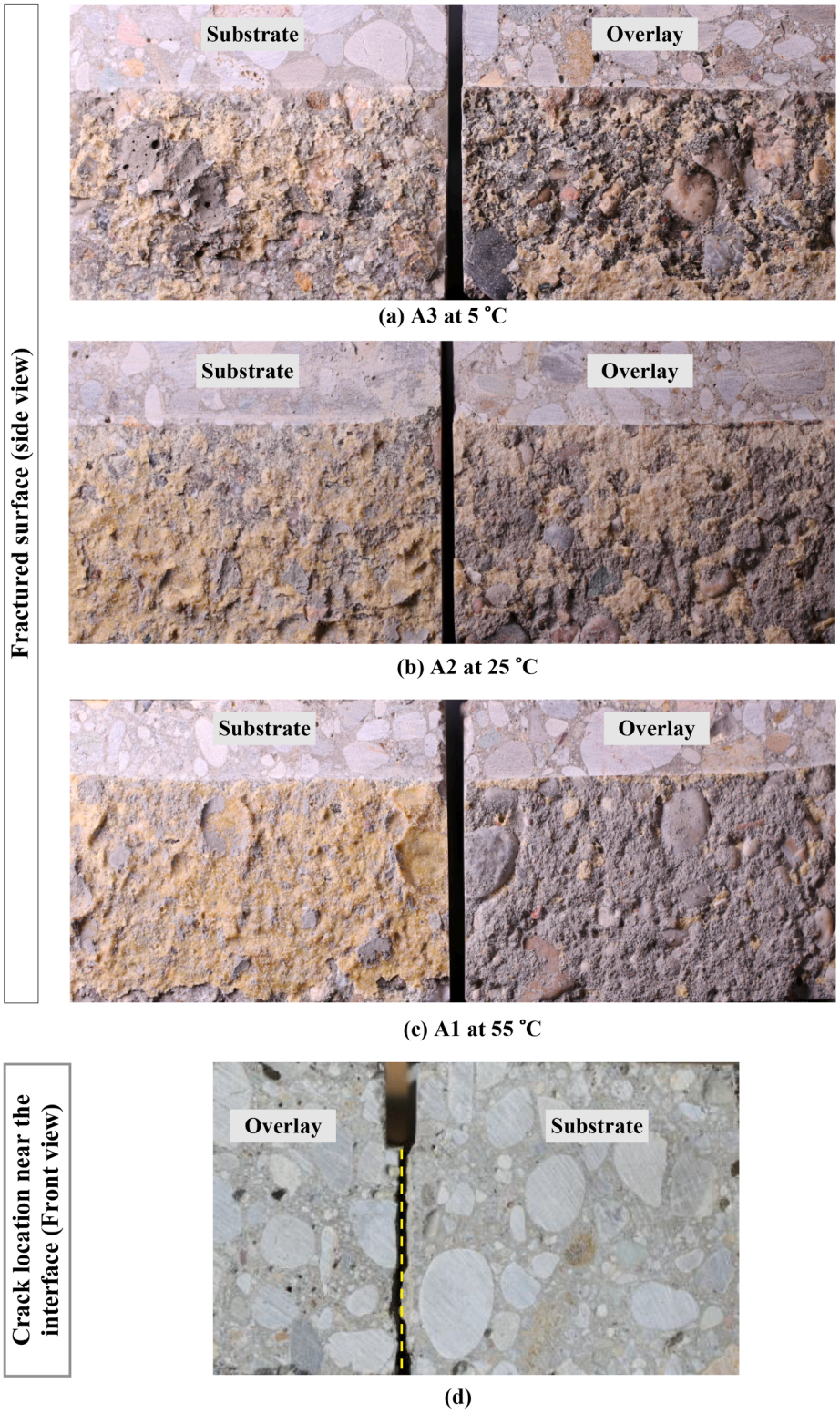

Fig. 14. Representative post-mortem bi-surface shear test samples. The adhesive failure includes three failure paths, namely interfacial failure between the epoxy layer and overlay (A1), serrated interfacial failure (A2), and alternating crack (A3). Figure (d) shows the crack location in the adhesive failure (front view). The yellow dashed line highlights the interface location.

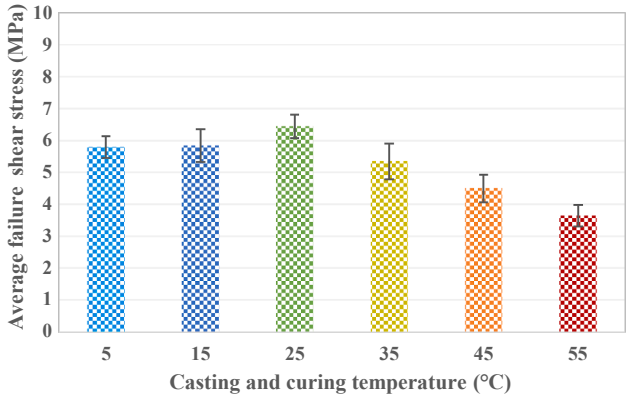

Fig. 15. Average shear strength measured with bi-surface shear test function of casting and curing temperature. Error bars represent standard deviation.

Table 11
Analysis of Variance (ANOVA) of bi-surface shear test results.

Source of Variation	*SS*	*df*	*MS*	*F*	*P-value*	F_{crit}
Between Groups	15.7	5	3.1	3.6	0.03	3.1
Within Groups	10.4	12	0.9			
Total	26.1	17				

SS: sum of squares; df: degrees of freedom; MS: mean square; F: local factor; p-value: probability value; Fc: critical factor

Table 12
Tukey's pairwise statistical analysis of bi-surface shear test results.

	Absolute difference					
	T5	T15	T25	T35	T45	T55
T5	–	0.04	0.7	0.5	1.3	**2.2***
T15		–	0.6	0.5	1.3	**2.2***
T25			–	1.1	1.9	**2.8***
T35				–	0.9	1.7
T45					–	0.9
T55						–

* Significant difference

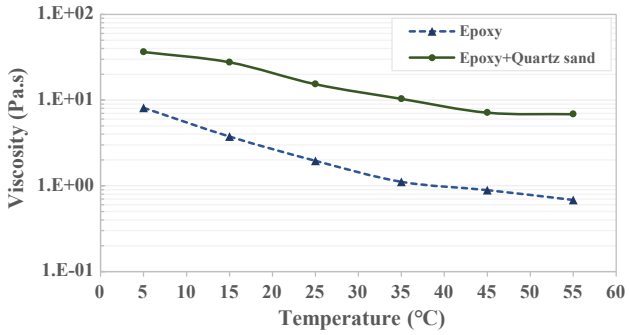

Fig. 16. Viscosity of epoxy and epoxy-quartz sand measured at the shear rate of 50 s^{-1} function of casting temperature.

temperature, i.e. 5 and 15 °C, the initial and final setting of cement paste happen while the epoxy is still in the early stages of curing (<50% degree of curing). However, at high temperature (45 and 55 °C), epoxy 90% degree of curing is achieved before the cement paste even starts to

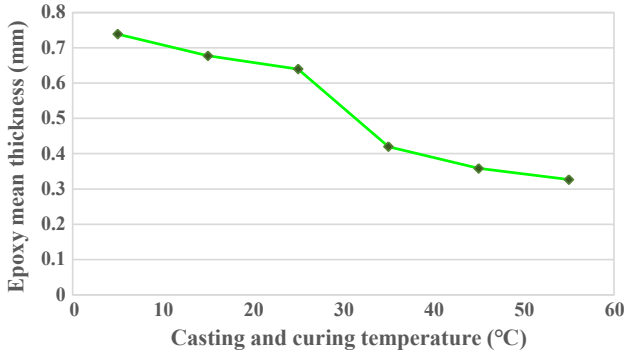

Fig. 17. Epoxy mean thickness after final curing function of casting and curing temperature.

set. For instance, the epoxy setting is nearly completed in 45 min at 55 °C while the cement paste initial setting time is 5 h and 45 min.

These graphs confirm that when specimen are casted and cured at 35, 45 and 55 °C, the epoxy sets before hydration products have had time to form. This prevents newly formed epoxy molecules to create specific interactions with hydrated cement (specifically C-S-H and Portlandite) [65]. This early setting of epoxy results in a weak bonding between epoxy and cement, confirmed by the adhesive failures observed in samples cured at these temperatures. Indeed, epoxy adhesive layer preferentially debonded from the overlay in all cases (see Fig. 23 and Fig. 24). Considering this evidence and the significant changes in setting times with temperature, the authors believe that the differential setting time is the most important factor explaining the decrease of bonding strength with increasing temperature.

These results give us key information on promising avenues to optimize epoxy-concrete bond performance. The main two avenues are either controlling the temperature during casting and curing, or better matching the epoxy and cement setting times. Specifically, the substrate temperature at the time of overlay pouring is recommended not to exceed 35 °C. Thus, in case of severe sunlight exposure, the substrate surface should be protected from getting hot several hours prior to epoxy/overlay application, using sun-shade covers. Casting at night/dawn is another option. Moreover, the temperature of both adhesive and concrete overlay components should also be kept below 35 °C when possible.

In addition to temperature control, the significant differential setting times in hot conditions could be mitigated by either accelerating the cement hydration or retarding the epoxy setting. Rapid hardening cement or chemical accelerators can be used to shorten the setting of cement and cement-based concrete. Also, introducing the gel time retarding agents into the epoxy adhesive would provide a more gradual hardening of the epoxy and hence a better time overlapping with cement setting.

Further studies are required to investigate the effect of those admixtures on the properties and bond performance of concrete-concrete composites, but are beyond the scope of this study.

4. Conclusion

In this study, the effect of casting and curing temperature on the interfacial bond strength of epoxy bonded concretes was investigated. For this purpose, six different temperatures, between 5 and 55 °C, were used to represent a wide range of climatic conditions at which epoxy bonded concrete composites are typically built. Based on the experimental results, the following observations were made:

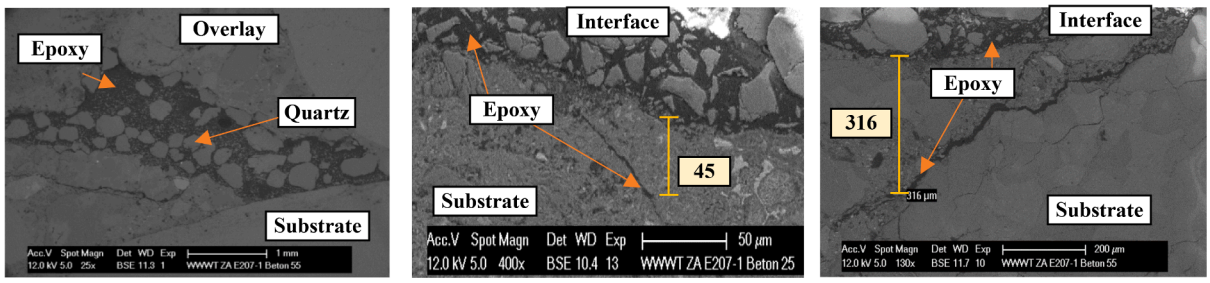

Fig. 18. Back-scattered electron images of epoxy-bonded concrete-concrete interface: **(a)** interfacial area filled with epoxy-quartz sand; Epoxy penetration into the concrete substrate for the samples cast and cured at **b)** 25 °C, and **c)** 55 °C.

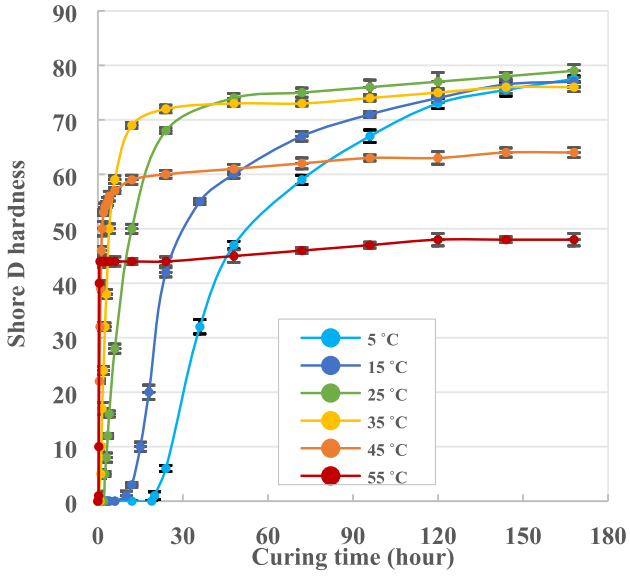

Fig. 19. Development of epoxy shore D hardness function of casting and curing temperature. Error bars represent the standard variation.

- The casting and curing temperature highly impacts the performance of epoxy bonded concretes. Increasing the temperature from 5 to 55 °C results in lowering the interfacial bond strength by 64% in direct tension, by 65% in Mode I fracture energy, and by 37% in pure shear.
- A greater number of cohesive failures were observed in the samples cast and cured at low temperatures, confirming their superior interfacial bond strength.

Investigating further the reasons behind the measurements and failure modes, three main factors contributing to the decreased interfacial bond strength with increasing casting and curing temperature were identified. They are presented below in order of importance:

- The setting of epoxy at high temperatures (35, 45 and 55 °C) was measured to be considerably faster than the setting of cement at these temperatures, preventing the development of interactions between epoxy and cement in the overlay. Indeed, when cement starts setting at 35 °C, our results show that the epoxy is already more than 80% reacted, and at 45 and 55 °C, it is more than 90% reacted. Post-mortem sample observations confirm this hypothesis, showing that fractures occur along the epoxy/overlay interface in all cases. The significant differential setting time between the epoxy and fresh overlay is considered as a key factor negatively impacting the interfacial bond strength of epoxy bonded concretes.
- The thickness of epoxy layer between the two concrete slabs was carefully measured and was lower when the composite was prepared at higher temperature. Indeed, between samples cured at 5 °C and

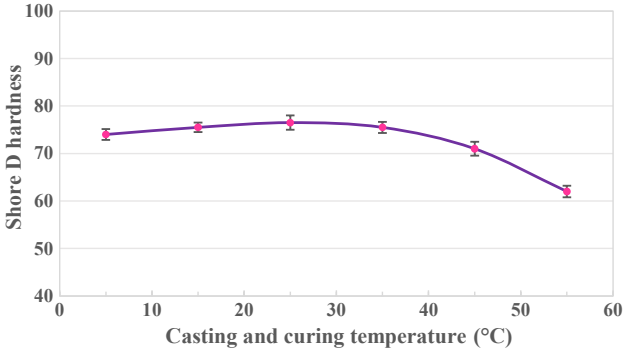

Fig. 20. Shore D hardness of epoxy measured at room temperature after 28 days of curing (7 days temperature curing plus 21 days lab ambient condition curing), as a function of casting and curing temperature. Error bars represent the standard variation.

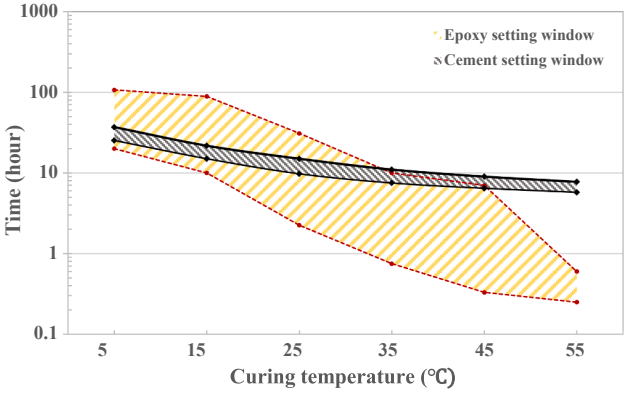

Fig. 21. Variation of epoxy and cement paste setting times function of casting and curing temperature.

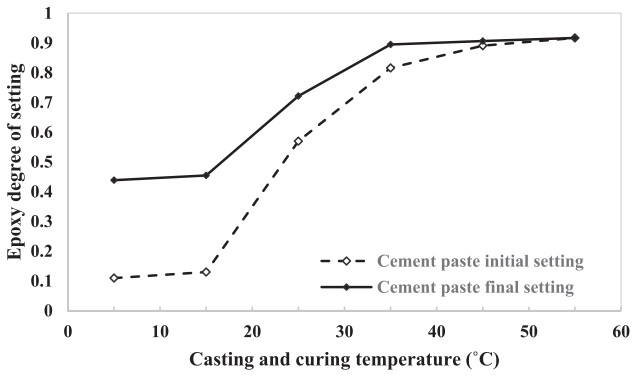

Fig. 22. Epoxy degree of setting at the time of occurrence of cement paste initial and final setting function of casting and curing temperature.

cured at 55 °C, the average epoxy layer thickness decreases by a factor more than 2. This is explained by the lower viscosity of epoxy at higher temperature, enabling deeper penetration into microcracks and pores of the concrete substrate, resulting in weaker interfacial adhesion and bond strength (also confirmed by SEM images).

- The surface hardness measurement of the epoxy revealed that the 28-day shore D hardness of the high temperature cured epoxy samples is lower (up to 18%) than the ones cured at low temperatures. The inferior mechanical properties of epoxy at high curing temperatures may be another reason behind the lower interfacial bond strength of epoxy-bonded concretes.

CRediT authorship contribution statement

Dana Daneshvar: Writing - original draft, Investigation, Formal analysis, Methodology, Writing - review & editing, Visualization. **Karl Deix:** Conceptualization, Investigation, Resources. **Agathe Robisson:** Supervision, Funding acquisition, Project administration, Conceptualization, Investigation, Writing - review & editing.

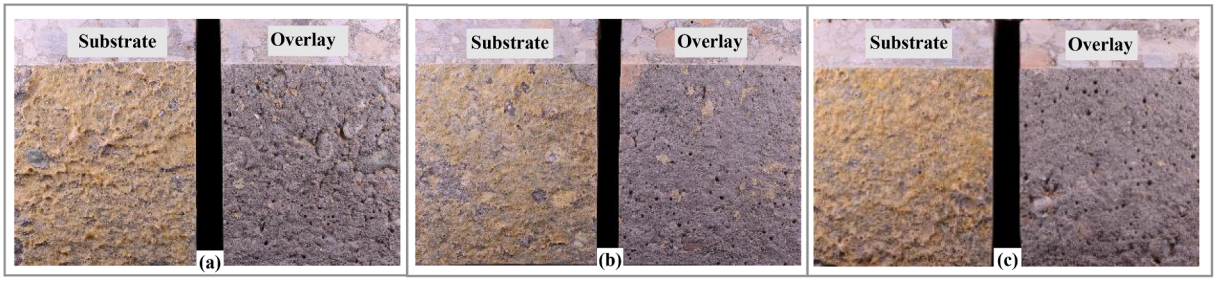

Fig. 23. Typical fractured surface of the WST samples cast and cured at: **(a)** 35 °C; **(b)** 45 °C; **(c)** 55 °C.

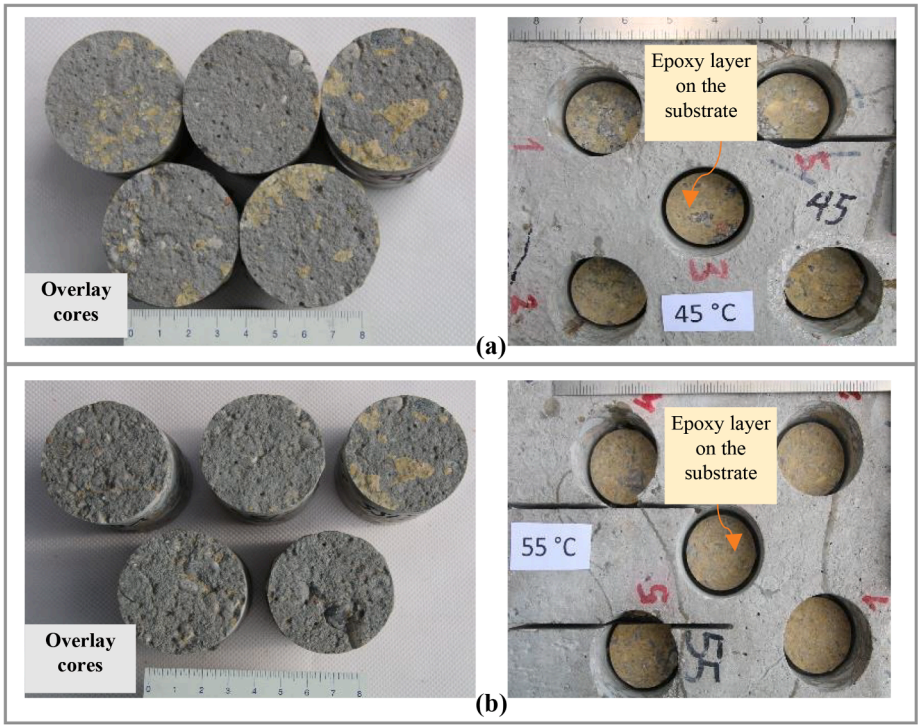

Fig. 24. Typical fractured surface of the pull-off samples cast and cured at: **(a)** 45 °C; **(b)** 55 °C.

Declaration of Competing Interest

The authors declare that they have no known competing financial interests or personal relationships that could have appeared to influence the work reported in this paper.

Acknowledgment

The authors thank Österreichische Bautechnik Vereinigung (ÖBV) and Österreichische Forschungsförderungsgesellschaft (FFG) for their support (Project number: 870962).

The authors acknowledge TU Wien Bibliothek for financial support through its Open Access Funding Programme.

References

[1] D.S. Santos, P.M.D. Santos, D. Dias-Da-Costa, Effect of surface preparation and bonding agent on the concrete-to-concrete interface strength, Constr. Build. Mater. 37 (2012) 102–110, https://doi.org/10.1016/j.conbuildmat.2012.07.028.
[2] M.A. Issa, C.L.R. do Valle, H.A. Abdalla, S. Islam, M.A. Issa, Performance of Transverse Joint Grout Materials in Bridge Deck Systems, PCI J. 48 (2003) 92–103.
[3] R.T.L. Allen, S.C. Edwards, D.N. Shaw, Repair of Concrete Structures, CRC Press, 1992.
[4] Y. He, X. Zhang, R.D. Hooton, X. Zhang, Effects of interface roughness and interface adhesion on new-to-old concrete bonding, Constr. Build. Mater. 151 (2017) 582–590, https://doi.org/10.1016/j.conbuildmat.2017.05.049.
[5] P.H. Emmons, Concrete Repair and Maintenance Illustrated, R. S. Means Company, MA, 1994.
[6] P.M.D. Santos, E.N.B.S. Júlio, A state-of-the-art review on roughness quantification methods for concrete surfaces, Constr. Build. Mater. 38 (2013) 912–923, https://doi.org/10.1016/j.conbuildmat.2012.09.045.
[7] M. Li, V.C. Li, Behavior of ECC-concrete layered repair system under drying shrinkage conditions.pdf.pdf, Restor. Build. Monum. (2006) 143–160.
[8] L. Courard, T. Piotrowski, A. Garbacz, Near-to-surface properties affecting bond strength in concrete repair, Cem. Concr. Compos. 46 (2014) 73–80, https://doi.org/10.1016/j.cemconcomp.2013.11.005.
[9] Eduardo N.B.S Júlio, Fernando A.B Branco, Vítor D Silva, Concrete-to-concrete bond strength. Influence of the roughness of the substrate surface, Constr. Build. Mater. 18 (9) (2004) 675–681, https://doi.org/10.1016/j.conbuildmat.2004.04.023.
[10] M. Frigione, M.A. Aiello, C. Naddeo, Water effects on the bond strength of concrete/concrete adhesive joints, Constr. Build. Mater. 20 (10) (2006) 957–970, https://doi.org/10.1016/j.conbuildmat.2005.06.015.
[11] Jian Zhou, Guang Ye, Erik Schlangen, Klaas van Breugel, Modelling of stresses and strains in bonded concrete overlays subjected to differential volume changes, Theor. Appl. Fract. Mech. 49 (2) (2008) 199–205, https://doi.org/10.1016/j.tafmec.2007.11.006.
[12] Bassam A. Tayeh, B.H. Abu Bakar, M.A. Megat Johari, Characterization of the interfacial bond between old concrete substrate and ultra high performance fiber concrete repair composite, Mater. Struct. Constr. 46 (5) (2013) 743–753, https://doi.org/10.1617/s11527-012-9931-1.
[13] H. Huang, Y. Yuan, W. Zhang, Z. Gao, Bond behavior between lightweight aggregate concrete and normal weight concrete based on splitting-tensile test, Constr. Build. Mater. 209 (2019) 306–314, https://doi.org/10.1016/j.conbuildmat.2019.03.125.
[14] Yang Zhang, Ping Zhu, Zhaoqian Liao, Lianhua Wang, Interfacial bond properties between normal strength concrete substrate and ultra-high performance concrete as a repair material, Constr. Build. Mater. 235 (2020) 117431, https://doi.org/10.1016/j.conbuildmat.2019.117431.
[15] Eduardo N.B.S. Júlio, Fernando A.B. Branco, Vítor D. Silva, Jorge F. Lourenço, Influence of added concrete compressive strength on adhesion to an existing concrete substrate, Build. Environ. 41 (12) (2006) 1934–1939, https://doi.org/10.1016/j.buildenv.2005.06.023.
[16] H. Fernandes, V. Lúcio, A. Ramos, Strengthening of RC slabs with reinforced concrete overlay on the tensile face, Eng. Struct. 132 (2017) 540–550, https://doi.org/10.1016/j.engstruct.2016.10.011.
[17] Alireza Valikhani, Azadeh Jaberi Jahromi, Islam M. Mantawy, Atorod Azizinamini, Experimental evaluation of concrete-to-UHPC bond strength with correlation to surface roughness for repair application, Constr. Build. Mater. 238 (2020) 117753, https://doi.org/10.1016/j.conbuildmat.2019.117753.
[18] Kaihua Liu, Chaoying Zou, Jiachuan Yan, Shear transfer behavior between substrate recycled aggregate concrete and new natural aggregate concrete, Struct. Concr. 22 (2) (2021) 1022–1036, https://doi.org/10.1002/suco.v22.210.1002/suco.201900570.
[19] Adnan Çolak, Turgay Çoşgun, Ahmet E. Bakırcı, Effects of environmental factors on the adhesion and durability characteristics of epoxy-bonded concrete prisms, Constr. Build. Mater. 23 (2) (2009) 758–767, https://doi.org/10.1016/j.conbuildmat.2008.02.013.
[20] Hongguang Zhu, Jingchong Fan, Cheng Yi, Hongqiang Ma, Hongyu Chen, Jing Shi, Xiaonan Xu, Characterization of freeze-thaw resistance of new-to-old concrete based on the ultrasonic pulse velocity method, J. Test. Eval. 49 (1) (2021) 20190639, https://doi.org/10.1520/JTE2101-EB10.1520/JTE20190639.
[21] Gengying Li, A new way to increase the long-term bond strength of new-to-old concrete by the use of fly ash, Cem. Concr. Res. 33 (6) (2003) 799–806, https://doi.org/10.1016/S0008-8846(02)01064-5.
[22] E. N. B. S. Júlio F. A. B. Branco V. D. Silva Concrete-to-concrete bond strength: Influence of an epoxy-based bonding agent on a roughened substrate surface Mag. Concr. Res. 57 8 2005 463 468 10.1680/macr.2005.57.8.463.
[23] J. C. T. S. Clímaco P. E. Regan Evaluation of bond strength between old and new concrete in structural repairs Mag. Concr. Res. 53 6 2001 377 390 10.1680/macr.2001.53.6.377.
[24] G.H. Ahmed, O.Q. Aziz, Shear behavior of dry and epoxied joints in precast concrete segmental box girder bridges under direct shear loading, Eng. Struct. 182 (2019) 89–100, https://doi.org/10.1016/j.engstruct.2018.12.070.
[25] A.M. Diab, A.E.M. Abd Elmoaty, M.R. Tag Eldin, Slant shear bond strength between self compacting concrete and old concrete, Constr. Build. Mater. 130 (2017) 73–82, https://doi.org/10.1016/j.conbuildmat.2016.11.023.
[26] J. Yeon, Y. Song, K.K. Kim, J. Kang, Effects of epoxy adhesive layer thickness on bond strength of joints in concrete structures, Materials (Basel). 12 (2019) 1–10, https://doi.org/10.3390/ma12152396.
[27] Christoph Czaderski, Enzo Martinelli, Julien Michels, Masoud Motavalli, Effect of curing conditions on strength development in an epoxy resin for structural strengthening, Compos. Part B Eng. 43 (2) (2012) 398–410, https://doi.org/10.1016/j.compositesb:2011.07.006.
[28] O. Moussa, A.P. Vassilopoulos, J. De Castro, T. Keller, Early-age tensile properties of structural epoxy adhesives subjected to low-temperature curing, Int. J. Adhes. Adhes. 35 (2012) 9–16, https://doi.org/10.1016/j.ijadhadh.2012.01.023.
[29] G.C. Mays, A.R. Hutchinson (Eds.), Adhesives in Civil Engineering, Cambridge University Press, 1992.
[30] Erol Sancaktar, Hooshang Jozavi, Robert M. Klein, The Effects of Cure Temperature and Time on the Bulk Tensile Properties of a Structural Adhesive, J. Adhes. 15 (3-4) (1983) 241–264, https://doi.org/10.1080/00218468308073230.
[31] R. J. C. Carbas E. A. S. Marques L. F. M. da Silva A. M. Lopes Effect of cure temperature on the glass transition temperature and mechanical properties of epoxy adhesives J. Adhes. 90 1 2014 104 119 10.1080/00218464.2013.779559.
[32] M. S. Islam K. L. Pickering N. J. Foreman Curing kinetics and effects of fibre surface treatment and curing parameters on the interfacial and tensile properties of hemp/epoxy composites J. Adhes. Sci. Technol. 23 16 2009 2085 2107 10.1163/016942409X12526743387962.
[33] Amir Malakooti, Hesham Abdualla, Sajed Sadati, Halil Ceylan, Sunghwan Kim, Kristen Cetin, Experimental and theoretical characterization of electrodes on electrical and thermal performance of electrically conductive concrete, Compos. Part B Eng. 222 (2021) 109003, https://doi.org/10.1016/j.compositesb:2021.109003.
[34] I. Soroka, D. Ravina, Hot weather concreting with admixtures, Cem. Concr. Compos. 20 (2-3) (1998) 129–136, https://doi.org/10.1016/S0958-9465(98)80005-X.
[35] Amir Malakooti, Wei Shen Theh, S.M. Sajed Sadati, Halil Ceylan, Sunghwan Kim, Mani Mina, Kristen Cetin, Peter C. Taylor, Design and Full-scale Implementation of the Largest Operational Electrically Conductive Concrete Heated Pavement System, Constr. Build. Mater. 255 (2020) 119229, https://doi.org/10.1016/j.conbuildmat.2020.119229.
[36] Knut O. Kjellsen, Rachel J. Detwiler, Odd E. Gjørv, Development of Microstructures in Plain Cement Pastes Hydrated at different temperatures, Cem. Concr. Res. 21 (1) (1991) 179–189.
[37] Y. Richard Kim, Youngguk Seo, Mark King, Mostafa Momen, Dynamic modulus testing of asphalt concrete in indirect tension mode, Transp. Res. Rec. 1891 (1) (2004) 163–173, https://doi.org/10.3141/1891-19.
[38] Xiangen Wang, Halwan Alfisa Saifullah, Hiroki Nishikawa, Kenichiro Nakarai, Effect of water–cement ratio, aggregate type, and curing temperature on the fracture energy of concrete, Constr. Build. Mater. 259 (2020) 119646, https://doi.org/10.1016/j.conbuildmat.2020.119646.
[39] L. Fan, Z. Zhang, Y. Yu, P. Li, T. Cosgrove, Effect of elevated curing temperature on ceramsite concrete performance, Constr. Build. Mater. 153 (2017) 423–429, https://doi.org/10.1016/j.conbuildmat.2017.07.050.
[40] E.B. Nelson, M. Michaux, Well Cementing: 2.Chemistry and characterization of Portland cement, 2006.
[41] E. Gallucci, X. Zhang, K.L. Scrivener, Effect of temperature on the microstructure of calcium silicate hydrate (C-S-H), Cem. Concr. Res. 53 (2013) 185–195, https://doi.org/10.1016/j.cemconres.2013.06.008.
[42] Fathollah Sajedi, Hashim Abdul Razak, Effects of curing regimes and cement fineness on the compressive strength of ordinary Portland cement mortars, Constr. Build. Mater. 25 (4) (2011) 2036–2045, https://doi.org/10.1016/j.conbuildmat.2010.11.043.
[43] Y. Huang, G. Liu, S. Huang, R. Rao, C. Hu, Experimental and finite element investigations on the temperature field of a massive bridge pier caused by the hydration heat of concrete, Constr. Build. Mater. 192 (2018) 240–252, https://doi.org/10.1016/j.conbuildmat.2018.10.128.
[44] Yogiraj Sargam, Mahmoud Faytarouni, Kyle Riding, Kejin Wang, Charles Jahren, Jay Shen, Predicting thermal performance of a mass concrete foundation – A field monitoring case study, Case Stud. Constr. Mater. 11 (2019) e00289, https://doi.org/10.1016/j.cscm.2019.e00289.
[45] S. Swaddiwudhipong, D. Chen, M.H. Zhang, Simulation of the exothermic hydration process of Portland cement, Adv. Cem. Res. 14 (2) (2002) 61–69, https://doi.org/10.1680/adcr.2002.14.2.61.

[46] S. K. Ha S. Na Y. K. Bang H. K. Lee An experimental study on sag-resistance ability and applicability of sprayed FRP system on vertical and overhead concrete surfaces Mater. Struct. Constr. 48 1-2 2015 21 33 10.1617/s11527-013-0165-7.
[47] A.R. Akisanya, N.A. Fleck, Fracture of Adhesive Joints, Int. J. Fract. 58 (1992) 93–114.
[48] A. Momayez, M.R. Ehsani, A.A. Ramezanianpour, H. Rajaie, Comparison of methods for evaluating bond strength between concrete substrate and repair materials, Cem. Concr. Res. 35 (4) (2005) 748–757, https://doi.org/10.1016/j.cemconres.2004.05.027.
[49] H.N. Linsbauer, E.K. Tschegg, Fracture energy determination of concrete with cube-shaped specimens, Zement Und Bet. 31 (1986) 38–40.
[50] E. Brühwiler, F.H. Wittmann, The wedge splitting test, a new method of performing stable fracture mechanics tests, Eng. Fract. Mech. 35 (1-3) (1990) 117–125, https://doi.org/10.1016/0013-7944(90)90189-N.
[51] E.K. Tschegg, K.T. Fendt, Ch. Manhart, H. Harmuth, Uniaxial and biaxial fracture behaviour of refractory materials, Eng. Fract. Mech. 76 (14) (2009) 2249–2259, https://doi.org/10.1016/j.engfracmech.2009.07.011.
[52] E.K. Tschegg, New equipments for fracture tests on concrete, Materialpruefung. 33 (1991) 338–343.
[53] A. Momayez A.A. Ramezanianpour H. Rajaie M.R. Ehsani Bi-surface shear test for evaluating bond between existing and new concrete ACI Mater. J. 101 2004 99 106 https://doi.org/10.14359/13045.
[54] Zhipeng Ran, Xiaobing Liu, Xiaolian Jiang, Yeping Wu, Hong Liao, Study on curing kinetics of epoxy-amine to reduce temperature caused by the exothermic reaction, Thermochim. Acta. 692 (2020) 178735, https://doi.org/10.1016/j.tca.2020.178735.
[55] EN 196-3, Methods of testing cement–Part 3: Determination of setting times and soundness, (2016).
[56] Sidney Diamond, The microstructure of cement paste and concrete - A visual primer, Cem. Concr. Compos. 26 (8) (2004) 919–933, https://doi.org/10.1016/j.cemconcomp.2004.02.028.
[57] Paul Stutzman, Scanning electron microscopy imaging of hydraulic cement microstructure, Cem. Concr. Compos. 26 (8) (2004) 957–966, https://doi.org/10.1016/j.cemconcomp.2004.02.043.
[58] S. Jin, D. Gruber, H. Harmuth, Determination of Young's modulus, fracture energy and tensile strength of refractories by inverse estimation of a wedge splitting procedure, Eng. Fract. Mech. 116 (2014) 228–236, https://doi.org/10.1016/j.engfracmech.2013.11.010.
[59] Carlos A. Coronado, Maria M. Lopez, Experimental Characterization of Concrete-Epoxy Interfaces, J. Mater. Civ. Eng. 20 (4) (2008) 303–312.
[60] P.W. Birkeland, H.W. Birkeland, Connections in Precast Concrete Construction, J. Am. Concr. Institute, ACI, Proc. 63 (1966) 345–368.
[61] N. Randl, Investigations on transfer of forces between old and new concrete at different joint roughness, PhD thesis, University of Innsbruck, 1999.
[62] Camille A. Issa, Pauls Debs, Experimental study of epoxy repairing of cracks in concrete, Constr. Build. Mater. 21 (1) (2007) 157–163, https://doi.org/10.1016/j.conbuildmat.2005.06.030.
[63] H.J. Qi, K. Joyce, M.C. Boyce, Durometer hardness and the stress-strain behavior of elastomeric materials, Rubber Chem. Technol. 76 (2003) 419–435, https://doi.org/10.5254/1.3547752.
[64] K. Larson Can You Estimate Modulus From Durometer Hardness for Silicones ? 2016 Dow Corning Corp 1 6.
[65] Fatma Djouani, Carole Connan, Michel Delamar, Mohamed M. Chehimi, Karim Benzarti, Cement paste-epoxy adhesive interactions, Constr. Build. Mater. 25 (2) (2011) 411–423, https://doi.org/10.1016/j.conbuildmat.2010.02.035.